

# Correlation for Species Surface Concentration on a Hypersonic Stagnation Point with Mass Injection

Marc Ewenz Rocher <sup>\*</sup>, Tobias Hermann <sup>†</sup> and Matthew McGilvray <sup>‡</sup>  
*The University of Oxford, Department of Engineering, Osney Mead, The Southwell Building,  
Oxford OX2 0ES, United Kingdom*

Rowan Gollan <sup>§</sup>  
*School of Mechanical & Mining Engineering, The University of Queensland, Brisbane QLD 4072, Australia*

**This paper presents a correlation to obtain the surface species concentration on a stagnation point with mass injection for hypersonic flow. The correlation can be used to determine surface recombination heat fluxes and oxidation levels for ablatives or actively cooled heat shields in thermochemical equilibrium flow. It explicitly expresses the wall species concentration as a function of freestream conditions, coolant properties and the stagnation point geometry, revealing the direct effect of the above parameters on the desired quantity. The method was compared against the numerically obtained self-similar solution and showed an accuracy of  $\pm 4\%$ . The concentration depends on the boundary layer edge pressure, temperature and velocity gradient, as well as the wall temperature and injected mass flux. The molar mass and diffusion coefficient are further needed for scaling if the injected gas differs from the freestream gas.**

## Nomenclature

$B_h$	=	$\frac{F}{St_{h0}}$ , blowing parameter for heat transfer
$B_m$	=	$\frac{F}{St_{m0}}$ , blowing parameter for mass transfer
$B_{m,i}$	=	$\lambda_i B_m$
$c$	=	mass fraction
$c_p$	=	specific heat capacity, $\text{J kg}^{-1} \text{K}^{-1}$
$D$	=	mass diffusivity, $\text{m}^2 \text{s}^{-1}$
$F$	=	$\frac{\rho_w v_w}{\rho_e v_e}$ , blowing ratio
$Fn$	=	function of
$f'$	=	$\frac{u}{u_e}$ , normalized velocity

---

<sup>\*</sup>DPhil Candidate, Oxford Thermofluids Institute, University of Oxford, AIAA Member, marc.ewenzrocher@eng.ox.ac.uk.

<sup>†</sup>Departmental Lecturer, Oxford Thermofluids Institute, University of Oxford, AIAA Member.

<sup>‡</sup>Associate Professor, Oxford Thermofluids Institute, University of Oxford, AIAA Member.

<sup>§</sup>Lecturer, School of Mechanical and Mining Engineering.

$h$	=	specific enthalpy, $\text{Jkg}^{-1}$
$j$	=	mass flux, $\text{kgm}^{-2}\text{s}^{-1}$
$K_h$	=	heat transfer coefficient, $\text{Wm}^{-2}\text{K}^{-1}$
$K_m$	=	mass transfer coefficient, $\text{ms}^{-1}$
$k$	=	thermal conductivity, $\text{Wm}^{-1}\text{K}^{-1}$
$L$	=	characteristic length, m
$l$	=	$\frac{\rho\mu}{\rho_e\mu_e}$ , Chapman-Rubesin factor
$M$	=	molar mass or Mach number
$\dot{m}$	=	mass generation per unit area, $\text{kgm}^{-2}\text{s}^{-1}$
$m$	=	$\frac{\eta}{\Delta}$ , dimensionless y-coordinate
$Pr$	=	$\frac{c_p\mu}{k}$ , Prandtl number
$p$	=	pressure, Pa
$\dot{q}$	=	heat flux, $\text{Wm}^{-2}$
$R$	=	probehead hemisphere radius, m
$Re$	=	$\frac{\rho u L}{\mu}$ , Reynolds number
$r$	=	cylindrical radius of body, m
$Sc$	=	$\frac{\mu}{\rho D}$ , Schmidt number
$Sh$	=	$\frac{j_w}{-\rho_w D_w \frac{c_e - c_{w'}}{L}}$ , Sherwood number
$St_h$	=	$\frac{K_h}{\rho_e u_e c_{p,e}}$ , heat transfer Stanton number
$St_m$	=	$\frac{K_m}{u_e}$ , mass transfer Stanton number
$T$	=	temperature, K
$u$	=	x component of velocity, $\text{ms}^{-1}$
$v$	=	y component of velocity, $\text{ms}^{-1}$
$\dot{w}$	=	mass generation per unit volume, $\text{kgm}^{-3}\text{s}^{-1}$
$x$	=	distance along surface, m
$y$	=	distance normal to surface, m
$\alpha$	=	$\frac{l}{Sc}$
$\beta$	=	generalized profile factor
$\Gamma_{c_p}$	=	$\frac{c_p}{c_{p,e}}$ , ratio of heat capacities
$\Delta$	=	effective film thickness
$\delta$	=	$\frac{\rho_e}{\rho}$ , density ratio
$\delta^*$	=	boundary layer thickness

$\eta$	=	defined by Eq. (8)
$\theta$	=	$\frac{T}{T_e}$ , normalized temperature
$\lambda_1$	=	scaling factor presented in Eq. (3)
$\lambda_2$	=	scaling factor for cases in Fig. 6 only
$\lambda_3$	=	scaling factor accounting for $Sc$
$\lambda_4$	=	scaling factor accounting for $Sc$ and $\frac{T_w}{T_e}$
$\lambda_5$	=	scaling factor for all cases
$\mu$	=	viscosity, Pa·s
$\xi$	=	defined by Eq. (8)
$\rho$	=	density, $\text{kgm}^{-3}$

#### Subscripts

0	=	no mass injection
adj	=	adjacent inner cell
$c$	=	coolant
$e$	=	boundary layer edge
ext	=	external gas
$i$	=	$i$ th component of mixture
inj	=	injected gas
$w$	=	wall
$\infty$	=	freestream

#### Superscript

'	=	derivative with respect to $\eta$
---	---	-----------------------------------

## I. Introduction

**H**YPERSONIC flight is experiencing a global renaissance due to growing scientific, economic and military interest. This has catalysed the research activity in the field in recent years. NASA's X-plane revival, the surge of suborbital passenger high-speed vehicle concepts and the SR-72 development manifest this trend. The stagnation points of these vehicles generate hot, often dissociated gas as they fly through the atmosphere. This results in high heat fluxes due to radiation, convection and surface recombination of atomic species. Surface reactions in the form of oxidation or nitration further endanger the aerodynamic and structural integrity of the vehicle. To ensure the safety of crew and payload, the vehicle must be protected from thermal and chemical attack [1]. For this purpose it is necessary to model the heat flux and mass transfer of freestream species at the wall and design suitable protection systems.

Heat flux has been studied extensively for stagnation points without mass injection [2, 3] and with mass injection (analytically [4], numerically [5] and experimentally [6]). Mass injection occurs passively during ablation or actively in transpiration cooling. Mass flux in contrast, has received less attention in the literature. The two detrimental effects associated with mass flux of freestream species to the wall are catalytic recombination and surface degradation through oxidation and nitration. The blowing of gaseous reaction products in ablatives, of an inert gas in transpiration cooling or any other form of mass injection at the stagnation point, will counteract this mass flux and reduce the amount of freestream gas at the wall.

To date, engineers have focused on the cooling effect of mass injection, but the operating temperature of most aerospace materials is constrained more stringently by oxidation than melting. Common and envisioned aerospace materials such as UHTCs [7–9] or C/C composites [10, 11] corrode at up to 2500 K below their melting temperature, restraining them from tapping their full refractory potential. Chemical attack also recesses the outer layer of ablatives. To model these processes, it is necessary to understand the freestream gas mass transfer at a stagnation point with mass injection. Beyond corrosion and chemical attack, knowledge of freestream activated species at a wall is required to predict catalytic heat flux. While the catalytic efficiency of surface materials remains an important subject of investigation [12, 13], little is known about the concentration of activated species at a given flight condition with stagnation point blowing. Fay and Riddell [2] predicted the recombination heat flux on a stagnation point in the absence of mass injection, but it is precisely this mechanism which shows a sharp decline in heat flux experimentally [6].

In order to predict the reduction in surface recombination and corrosion it is necessary to model the freestream mass transfer at a stagnation point with mass injection. This is commonly done numerically, by solving the self-similar boundary layer equations [14]. In heat transfer it is found that numerical and experimental results correlate well with the following equation, derived from film theory [4, 15]:

$$\frac{St_h}{St_{h0}} = \frac{\lambda B_h}{e^{\lambda B_h} - 1}, \quad (1)$$

where  $\lambda$  accounts for geometric effects and differences in coolant and boundary layer edge transport properties. The blowing parameter  $B_h = \frac{F}{St_{h0}}$  is composed of the blowing ratio  $F$  and the heat Stanton number for no mass injection  $St_{h0}$ . Unfortunately a simple heat-mass transfer analogy, replacing  $B_h$  with  $B_m = \frac{F}{St_{m0}}$  and  $St_h$  with  $St_m$ , does not lead to the desired result. The mass equivalent correlation simply does not correlate with numerically or experimentally obtained data. Ref. [16] introduced the following weighting factor

$$\frac{St_m}{St_{m0}} = \frac{\lambda_1 B_m}{e^{\lambda_1 B_m} - 1}, \quad (2)$$

$$\lambda_1 = 1.65 \left( \frac{M_{\text{air}}}{M_{\text{inj}}} \right)^{\frac{5}{6}}. \quad (3)$$

This is an empirical fit for air as the freestream gas. It explicitly shows the effect of two injectant parameters: the mass flow rate and the molecular mass. All other parameters, such as the wall to boundary layer edge temperature ratio, absolute wall temperature, diffusion coefficients, velocity gradient, are either neglected or their effect is lumped together in a numerical constant, which needs to be computed for each individual case. It is desirable to replace the numerical constants by an explicit function of said parameters. This would reduce time and complexity of the calculations and most importantly help engineers understand the underlying principles of stagnation point mass transfer when designing ablatives or transpiration cooled leading edges. It should also be noted that the above work assumed a constant heat capacity and derived the transport properties from kinetic theory, which leads to errors at the high temperatures encountered by ablatives and hypersonic stagnation points.

This paper presents a semi-analytical approach to obtain the mass transfer of freestream species at a stagnation point with mass injection. Starting with the conservation of mass, momentum, energy and species, the self-similar boundary layer equations are derived and validated against a full CFD solver. These analytical equations are then combined with thin film theory to obtain an explicit correlation for the species concentration and mass Stanton number at the surface.

## II. Analysis

### A. Governing equations

The flowfield around a hypersonic, axisymmetric stagnation point with mass injection is governed by the laminar boundary layer equations [17]

$$\frac{\partial(\rho ru)}{\partial x} + \frac{\partial(\rho rv)}{\partial y} = 0 \quad (4)$$

$$\rho u \frac{\partial u}{\partial x} + \rho v \frac{\partial u}{\partial y} = -\frac{dp}{dx} + \frac{\partial(\mu \frac{\partial u}{\partial y})}{\partial y} \quad (5)$$

$$\rho u \frac{\partial h}{\partial x} + \rho v \frac{\partial h}{\partial y} = \frac{\partial}{\partial y} \left( k \frac{\partial T}{\partial y} \right) + u \frac{\partial p}{\partial x} + \mu \left( \frac{\partial u}{\partial y} \right)^2 \quad (6)$$

$$\rho u \frac{\partial c_i}{\partial x} + \rho v \frac{\partial c_i}{\partial y} = \frac{\partial(D_i \rho \frac{\partial c_i}{\partial y})}{\partial y} + \dot{w}_i \quad (7)$$

where Eqs. (4-7) describe the conservation of mass, momentum, energy and species, respectively. It is possible to

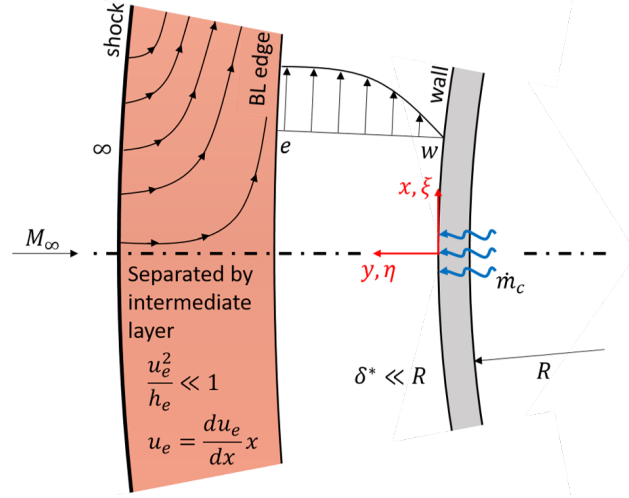


**Fig. 1 Sketch of a self-similar stagnation point, illustrating the assumptions made.**

transform these partial differential equations to a set of ordinary differential equations, in a procedure pioneered by Blasius in 1908 for incompressible flow across a flat plate and further developed for the hypersonic stagnation point by Dorodnitsyn [18] and Lees [19]. This transformation into non-dimensional space is desirable because it makes the solution self-similar. Self-similar theory makes the following assumptions, which are visualized in Figure 1:

- 1) the boundary layer edge and the shock are separated by an intermediate layer. This may be violated if the Reynolds number is too low, considering that the boundary layer thickness grows  $\propto \frac{1}{\sqrt{Re}}$ . For the cases considered in this work, the Reynolds number is large enough.
- 2) the boundary layer thickness is much smaller than the radius of curvature, such that most derivatives in  $\xi$  direction, along the surface, are negligible. The velocity gradient,  $\frac{du_e}{d\xi}$  is the exception.
- 3) the post shock kinetic energy is small compared to the total enthalpy  $\frac{u_e^2}{h_e} \ll 1$ , where  $e$  denotes the boundary layer edge conditions.
- 4) the flow outside the boundary layer edge is inviscid and incompressible. With this in mind, one can use the Falkner-Skan wedge flow solutions to obtain the boundary layer edge velocity,  $u_e = \frac{du_e}{dx} x$  [20].

Self-similar theory has been employed in the literature before, for instance to derive the stagnation point heat flux with no mass injection [2] and to numerically evaluate the velocity, temperature and concentration profiles of a transpiration cooled stagnation point in a perfect gas [14]. In the following, the self-similar equations for a stagnation point with blowing in an ideal gas are developed. The gas is assumed to be in thermochemical equilibrium.

## B. Boundary layer transformation and boundary conditions

The transformed coordinates are defined as follows:

$$\xi = \int_0^x \rho_e \mu_e u_e r^2 dx, \quad \eta = \frac{u_e r}{\sqrt{2\xi}} \int_0^y \rho dy, \quad (8)$$

with the corresponding derivatives

$$\frac{\partial}{\partial x} = \frac{\partial}{\partial \xi} \rho_e u_e \mu_e r^2 + \frac{\partial}{\partial \eta} \frac{\partial \eta}{\partial x}, \quad (9)$$

$$\frac{\partial}{\partial y} = \frac{\partial}{\partial \xi} (0) + \frac{\partial}{\partial \eta} \frac{u_e \rho r}{\sqrt{2\xi}}. \quad (10)$$

The resulting self-similar equations for a binary coolant-freestream mixture with no chemical reactions are

$$(lf'')' + ff'' + \frac{1}{2}(\delta - f'^2) = 0 \quad (11)$$

$$\left( \frac{\Gamma_{c_p} l}{Pr} \theta' \right)' + \Gamma_{c_p} f \theta' + \frac{l}{Sc} \left( \frac{c_{p;\text{inj}}}{c_{p;e}} - \frac{c_{p;\text{ext}}}{c_{p;e}} \right) c' \theta' = 0 \quad (12)$$

$$\left( \frac{l}{Sc} c' \right)' + f c' + \frac{\dot{w}_i}{2 \frac{du_e}{dx} \rho} = 0 \quad (13)$$

where  $f' = \frac{u}{u_e}$  denotes the velocity ratio,  $\theta = \frac{T}{T_e}$  the temperature ratio and  $c$  the coolant mass fraction. Please refer to Chapter 6.5 in Ref. [17] for a more extensive derivation of Eqs. (11-13). Note that  $\dot{w}_i$  accounts for the mass injection at the wall, for instance due to transpiration cooling.

The boundary conditions are defined next. A no-slip, fixed temperature condition is applied at the wall. The coolant concentration at the boundary layer edge is set to zero, yielding

$$f'_w = 0 \quad (14a)$$

$$\theta_w = \frac{T_w}{T_e} \quad (14b)$$

$$f'_e = 1 \quad (14c)$$

$$\theta_e = 1 \quad (14d)$$

$$c_e = 0 \quad (14e)$$

Furthermore, the integrated velocity function at the wall,  $f_w$ , is derived from the continuity equation using the stream functions, which are expressed in transformed coordinates using Eq. (10):

$$\frac{\partial \psi}{\partial y} = \rho u r = \rho f' u_e r = \frac{\partial \psi}{\partial \eta} \frac{u_e \rho r}{\sqrt{2\xi}}. \quad (15)$$

By inspection of Eq. (15)

$$\frac{\partial \psi}{\partial \eta} = \sqrt{2\xi} f' \quad (16)$$

and thus

$$\psi = \sqrt{2\xi} f \quad \frac{\partial \psi}{\partial \xi} = \sqrt{2\xi} \frac{\partial f}{\partial \xi} + \frac{1}{\sqrt{2\xi}} f. \quad (17)$$

The stream function is differentiated with respect to the streamwise distance  $x$  using Eq. (9):

$$\begin{aligned} \frac{\partial \psi}{\partial x} &= -\rho v r = \frac{\partial \psi}{\partial \xi} \rho_e u_e \mu_e r^2 + \frac{\partial \psi}{\partial \eta} \frac{\partial \eta}{\partial x} \\ &= \left( \sqrt{2\xi} \frac{\partial f}{\partial \xi} + \frac{1}{\sqrt{2\xi}} f \right) \rho_e u_e \mu_e r^2 \\ &\quad + \sqrt{2\xi} f' \frac{\partial \eta}{\partial x}. \end{aligned} \quad (18)$$

The derivatives in wall tangential ( $\xi$ ) direction can be neglected, as stated in section II.A. At the wall, Eq. (18) can be rearranged as follows, yielding the sixth boundary condition at the wall:

$$f_w = \frac{\rho_w v_w r \sqrt{2\xi}}{\rho_e u_e \mu_e r^2} = - \frac{\rho_w v_w}{\sqrt{2\rho_e \mu_e} \frac{du_e}{dx}}. \quad (19)$$

The concentration boundary condition is found by applying Eq. (7) at the wall:

$$(\rho v)_w \frac{\partial c_{i,w}}{\partial y} = \frac{\partial (D_i \rho \frac{\partial c_i}{\partial y})_w}{\partial y} + \dot{w}_i. \quad (20)$$

Equation (21) is found by integrating Eq. (20) with respect to  $y$ :

$$(\rho v c_i)_w = \left( D_i \rho \frac{\partial c_i}{\partial y} \right)_w + \dot{m}_i. \quad (21)$$

Note that  $\dot{w}_i = \frac{\partial \dot{m}_i}{\partial y}$  and  $\frac{\partial (\rho v c_i)_w}{\partial y} = (\rho v)_w \frac{\partial c_{i,w}}{\partial y}$ , as



$$\begin{aligned}
\frac{\partial(\rho v)_w}{\partial y} &= -\sqrt{2\rho_e\mu_e} \frac{du_e}{dx} \frac{\partial f_w}{\partial y} \\
&= -\sqrt{2\rho_e\mu_e} \frac{du_e}{dx} \frac{\partial \eta}{\partial y} \frac{\partial f_w}{\partial \eta} \\
&= -\sqrt{2\rho_e\mu_e} \frac{du_e}{dx} \sqrt{\frac{2\frac{du_e}{dx}}{\rho_e\mu_e}} \frac{\partial f_w}{\partial \eta} \\
&= -4 \frac{du_e}{dx} f'_w = -4 \frac{du_e}{dx} \left(\frac{u}{u_e}\right)_w = 0,
\end{aligned} \tag{22}$$

applying the no-slip condition  $\left(\frac{u}{u_e}\right)_w = 0$ . Defining  $c_{\text{inj}} = c$  and  $c_{\text{ext}} = 1 - c$  and using Eq. (21), the species continuity equations at the wall for the injected and the external flow in a binary mixture become

$$(\rho v c)_w = D_{12} \rho_w \left(\frac{\partial c}{\partial y}\right)_w + \dot{m}, \tag{23}$$

$$(\rho v)_w - (\rho v c)_w = -D_{12} \rho_w \left(\frac{\partial c}{\partial y}\right)_w, \tag{24}$$

respectively. The implicit assumption here is that the external flow does not enter the porous wall and that the mass flux  $\dot{m}$  crossing the surface consists purely of injected gas. This should not be confused with the assumption that the coolant concentration at the wall is 100%.

Adding Eqs. (23) and (24), it is apparent that  $\dot{m} = (\rho v)_w$ . Eq. (23) uses this expression for  $\dot{m}$  and is transformed into non-dimensional space to obtain a boundary condition for the concentration gradient at the wall:

$$\left(\frac{\partial c}{\partial \eta}\right)_w = \left(\frac{Sc}{l}\right)_w f_w (1 - c_w). \tag{25}$$

There are now 7 boundary conditions (Eqs. (14), (19) and (25)) for 7 unknowns  $f, f', f'', \theta, \theta', c, c'$  in Eqs. (11-13). The above set of equations constitutes a boundary value problem, which can be solved numerically. The velocity gradient is obtained from Modified Newtonian Theory [17], which is only applicable to hypersonic flows:

$$\frac{du_e}{dx} = \frac{1}{R} \sqrt{\frac{2(p_e - p_\infty)}{\rho_e}}. \tag{26}$$

For lower Mach numbers a correlation is provided in Ref. [21], however, the Mach number needs to be high enough for the post-shock flow to be assumed incompressible and thus for the Falkner-Skan solution to hold. Note that the diffusion coefficient was modelled using the Lennard-Jones parameters, as described in Chapter 17.3 of Ref. [22], while all other thermophysical properties were obtained from CEA2 [23].

### C. Validation with high-fidelity CFD solver

In this work, the validation of the self-similar method is undertaken by comparison with the high-fidelity CFD solver Eilmer 4 [24, 25]. This validation method was chosen due to the lack of experimental reference data in the literature. Figure 2 illustrates the setup of the CFD simulation. Since the modelled hemisphere is axisymmetric, the southern boundary has a no-slip condition. The western boundary is fitted to the shock, while the northern boundary assumes a supersonic outflow. The mass injection is modelled with a porous injection boundary condition, which works as follows:

- 1) At every time step, every interface along the boundary is assigned a pressure, temperature, concentration and velocity.
- 2) Pressure continuity is assumed and thus the pressure of the adjacent inner cell is assigned to the interface.
- 3) The coolant temperature is predefined and kept constant. The gas and the wall are assumed to have the same temperature.
- 4) The coolant concentration is solved using Eq. (23), noting that  $(\rho v)_w = \dot{m}$ . It is discretized as follows:

$$\left(\frac{\partial c}{\partial y}\right)_w = (c_w - 1) \frac{v_w}{D_{12}} \quad (27)$$

$$\frac{c_{\text{adj}} - c_w}{\Delta x} = (c_w - 1) \frac{v_w}{D_{12}} \quad (28)$$

$$c_w = \frac{c_{\text{adj}} + \frac{v_w \Delta x}{D_{12}}}{1 + \frac{v_w \Delta x}{D_{12}}} \quad (29)$$

where  $c_{\text{adj}}$  is the coolant concentration of the adjacent inner cell and  $\Delta x$  the distance between the midpoints of the interface and the adjacent inner cell.

- 5) The normal velocity is calculated using the predefined injection mass flux and the density at the wall,  $v_w = \frac{\dot{m}_{\text{inj}}}{\rho_w}$ . The tangential velocity is set to zero to implement the no-slip condition.

Figure 4 compares the velocity, temperature and concentration profiles as computed by the self-similar solutions to the ones obtained by Eilmer 4. The test case featured a 25 mm radius hemispherical probehead in a Mach 7 air freestream, with  $p_\infty = 187.7$  Pa,  $u_\infty = 989$  m/s and  $T_\infty = 49.7$  K. The velocity gradient was 6% higher than predicted by Eq. (26), due to 3D effects and the geometry change caused by the injected gas. A value of  $\frac{du_e}{dx} = 23410\text{s}^{-1}$  was obtained and used in the self-similar solution as well. Table 1 summarises the properties of the injected coolants. The mesh was clustered near the shock and boundary layer, as illustrated in Fig. 3. The solution converged at a mesh size of  $10\ \mu\text{m}$  normal to the wall. The mesh size was decreased further and the results compared to confirm mesh independence. A blend of the low dissipation AUSMDV scheme for the regions away from shocks and a more diffusive Hanel-Schwane-Seider scheme for the interfaces near shocks was employed as flux calculator. Figures 2 and 3 depict the coolant concentration around the whole hemisphere and just in the stagnation region, respectively, for case 1. The

**Table 1** Parameters of the validation test cases. All cases had an air freestream,  $p_e = 11.9$  kPa and  $T_w = 300$  K.

Case	Inj	$T_e/K$	$\dot{m}/(\frac{\text{kg}}{\text{m}^2\text{s}})$
1	$N_2$	537	0.2
2	$N_2$	1800	0.2
3	Ne	537	0.2
4	Ar	537	0.2

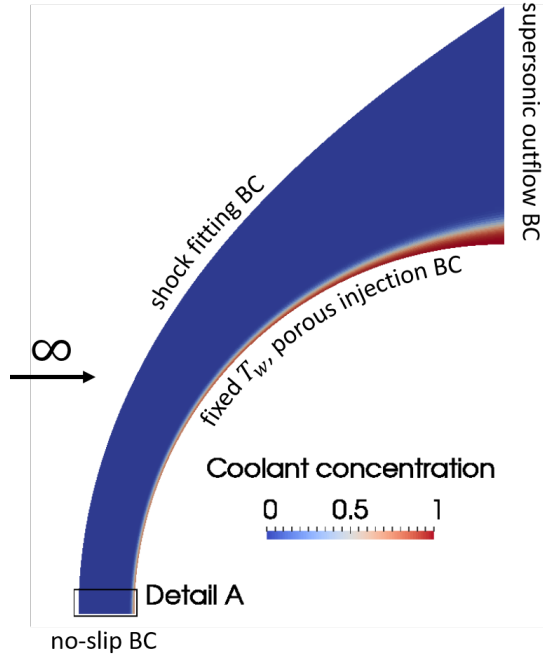


**Fig. 2** Eilmer 4 result, depicting the coolant concentration for the test case shown in Table 1.

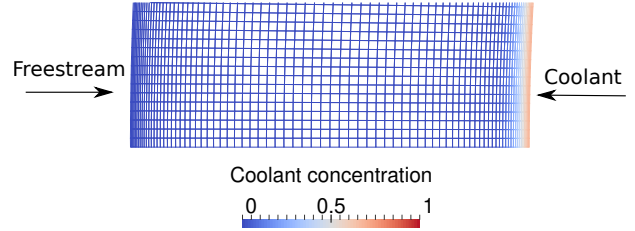


**Fig. 3** Wireframe of Detail A from Fig. 2, illustrating the mesh size and coolant concentration near the stagnation point.

model compares well with the CFD solver, despite its simplifying assumptions (see section II.A). Cases with very dissimilar coolant and freestream gases display a larger discrepancy than a homogeneous boundary layer. The error for all three profiles is within 5% for all conditions described in Table 1. Thus, the self-similar solutions are deemed suitable to numerically validate the analytical solutions derived in the following section.

#### D. Mass transfer coefficient for no mass injection and fixed $c_w$

Before considering a stagnation point with mass injection, the mass transfer of freestream species to the surface in the absence of blowing is reviewed. The same approach that Fay-Riddell used to derive the heat transfer on a stagnation [2] will be employed here to find its mass transfer equivalent. The mass flux of freestream gas at the wall is given as

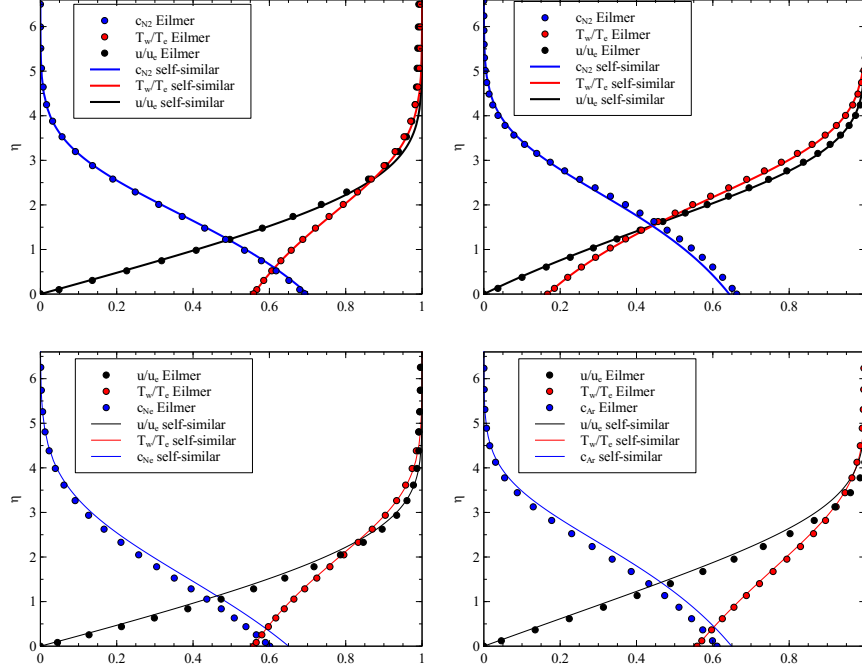


**Fig. 4** Comparison of the self-similar solution to the high fidelity CFD solver result for test cases in Table 1. Cases 1-4 are shown in chronological order from top left to bottom right.

$$j_w = -\rho_w D_{12} \left( \frac{\partial c}{\partial y} \right)_w, \quad (30)$$

which can be transformed into non-dimensional space and simplified using the definition of  $\xi$  (Eq. (8)):

$$j_w = -\rho_w D_{12} \sqrt{\frac{2\rho_w}{\mu_w} \frac{\partial u_e}{\partial x}} \left( \frac{\partial c}{\partial \eta} \right)_w. \quad (31)$$

Analogously to the heat transfer parameter  $\frac{Nu}{\sqrt{Re}}$ , the mass transfer parameter can be defined as [20]

$$\begin{aligned} \frac{Sh}{\sqrt{Re}} &= \frac{j_w}{-\rho_w D_{12} (c_e - c_w)/x} \sqrt{\frac{\mu_w}{\rho_w u_e x}} \\ &= \frac{Sc_w}{c_w} \frac{j_w}{\sqrt{\mu_w \rho_w} \frac{\partial u_e}{\partial x}}. \end{aligned} \quad (32)$$

Note that  $c_e = 0$ , as defined in Eq. (14). Equation (32) is rearranged as follows:

$$j_w = \frac{Sh}{\sqrt{Re}} c_w \sqrt{\mu_w \rho_w} \frac{\partial u_e}{\partial x} \frac{1}{Sc_w}. \quad (33)$$

By inspection with Eq. (31), the mass transfer parameter for a stagnation point with no injection is

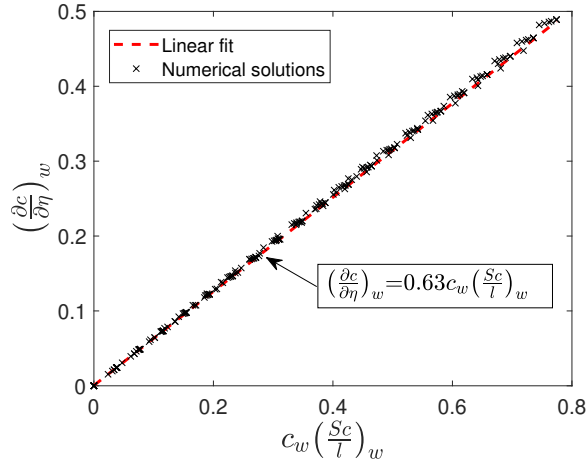


**Fig. 5 Results of the parameter study to obtain the factor  $K$ .**

**Table 2 Conditions of the parameter study to find  $K$ .**

#	Inj	Ext	$p_e/\text{kPa}$	$T_w/\text{K}$	$T_e/\text{K}$	$R/\text{mm}$
1	Air	Air	11.9	300	300	25
2	Air	Air	11.9	300	300	50
3	Air	Air	23.8	300	300	25
4	$N_2$	Air	11.9	300	515	25
5	Air	Air	11.9	300	1500	25
6	Air	Air	11.9	1000	1500	25
7	Air	Air	60	1000	2000	10
8	Ar	Ar	11.9	300	300	25
9	He	He	11.9	300	300	25
10	Ne	Ne	11.9	300	300	25
11	Xe	Xe	11.9	300	300	25

$$\frac{Sh}{\sqrt{Re}} = -\frac{\sqrt{2}}{c_w} \left( \frac{\partial c}{\partial \eta} \right)_w. \quad (34)$$

The concentration gradient at the wall,  $\left( \frac{\partial c}{\partial \eta} \right)_w$  for no mass injection is derived starting with the self-similar species conservation equation Eq. (13). Since  $f_w$  and  $\dot{w}$  are zero for no injection, it can be simplified as follows:

$$\left( \frac{l}{Sc} c' \right)' = 0 \quad (35a)$$

$$\left( \frac{\partial c}{\partial \eta} \right)_w = K \left( \frac{Sc}{l} \right)_w. \quad (35b)$$

The factor  $K$  is found to be  $K = 0.63c_w$  following a numerical parameter study, depicted in Fig. 5, including the conditions shown in Table 2. This correlation is only accurate if the coolant and freestream gas are identical or similar, such as  $N_2$  and air. The concentration gradient for a stagnation point with no mass injection is found to be

$$\left(\frac{\partial c}{\partial \eta}\right)_w = 0.63c_w \left(\frac{Sc}{l}\right)_w \quad (36)$$

and the mass transfer parameter becomes

$$\frac{Sh}{\sqrt{Re}} = 0.89 \left(\frac{Sc}{l}\right)_w. \quad (37)$$

The mass transfer rate simplifies to

$$j_w = 0.89 \frac{\rho_e \mu_e}{\sqrt{\rho_w \mu_w}} c_w \sqrt{\frac{\partial u_e}{\partial x}}. \quad (38)$$

Finally, the mass transfer coefficient for no mass injection, but a fixed  $c_w$ , is simply the mass transfer rate divided by the driving force, noting that  $c_e = 0$ ,

$$K_{m0} = \frac{j_w}{c_w - c_e} \quad (39a)$$

$$K_{m0} = 0.89 \frac{\rho_e \mu_e}{\sqrt{\rho_w \mu_w}} \sqrt{\frac{\partial u_e}{\partial x}}, \quad (39b)$$

and the corresponding Stanton number becomes

$$St_{m0} = 0.89 \frac{\rho_e \mu_e}{\sqrt{\rho_w \mu_w}} \sqrt{\frac{\partial u_e}{\partial x}} \frac{1}{u_e}. \quad (40)$$

### E. Film theory approach

This section attempts to derive  $St_m$  analytically using film theory. Film theory, firstly described in Ref. [15], predicts the ratio of mass transfer coefficients with mass injection,  $K_m$  to the mass transfer coefficient in the absence of mass injection,  $K_{m0}$ . It is less realistic than the boundary layer concept, but greatly simplifies the analysis of the mass transport between the freestream and the wall. It is shown that an equation of the form

$$\frac{d^2 \beta}{dm^2} - B_m \left(\frac{d\beta}{dm}\right) = 0, \quad (41)$$

with boundary conditions  $\beta = 0$  when  $m = 0$  and  $\beta = 1$  when  $m = 1$  has the following dimensionless gradient at the wall:

$$\left(\frac{\partial\beta}{\partial m}\right)_w = \frac{B_m}{e^{B_m} - 1}. \quad (42)$$

$\beta$  is the normalized velocity, temperature or concentration and is called generalized profile factor, while  $m$  is the normalized  $y$  coordinate. Furthermore, it is demonstrated that the ratio of non-dimensional gradients, corresponds to the ratio of mass transfer coefficients [15]

$$\frac{\left(\frac{\partial\beta}{\partial\eta}\right)_w}{\left(\frac{\partial\beta}{\partial\eta}\right)_{w;0}} = \frac{K_m}{K_{m;0}} = \frac{B_m \frac{\Delta_0}{\Delta}}{e^{B_m} - 1}, \quad (43)$$

where  $\frac{\Delta}{\Delta_0}$  denotes the ratio of film thicknesses with and without mass injection. Film theory assumes that this ratio is unity.

This paper presents a simplification which relates the above ratio of non-dimensional gradients directly to the surface concentration of external species. Using Eqs. (25) and (36):

$$\frac{\left(\frac{\partial\beta}{\partial\eta}\right)_w}{\left(\frac{\partial\beta}{\partial\eta}\right)_{w;0}} = \frac{\left(\frac{\partial c}{\partial\eta}\right)_w}{\left(\frac{\partial c}{\partial\eta}\right)_{w;0}} = \frac{f_w(1 - c_w)}{0.63c_w} \approx 1 - c_w. \quad (44)$$

The approximation holds well for all blowing rates considered in this study. The ratio  $\frac{f_w}{0.63c_w} \rightarrow 1$  for small blowing ratios can be inferred by setting the right hand side of Eq. (25) equal to that of Eq. (36). While Eq. (36) strictly speaking is only valid for no blowing, it is found that the above approximation is accurate for small to moderate mass fluxes. For large mass fluxes, which lead to  $\frac{K_m}{K_{m;0}} = 1 - c_w \ll 0.01$ , the approximation will not hold. However, the absolute difference to the correct value will be small. The following correlation is obtained when combining Eq. (43) and (44):

$$1 - c_w = \frac{B_m}{e^{B_m} - 1}, \quad (45)$$

with  $B_m$  defined as the blowing parameter for mass transfer.

In heat transfer it is common practice to denote the ratio of heat transfer coefficients as the ratio of Stanton numbers, as shown for instance in Ref. [26]. The Stanton number is the ratio of heat transfer at the surface to the thermal capacity of the passing fluid. Analogously, the mass transfer Stanton number,  $St_m$ , is defined as the ratio of mass transfer at the surface to the velocity of the passing fluid:  $St_m = \frac{K_m}{u_e}$ . Thus, Eq. (43) can be rewritten as

$$\frac{St_m}{St_{m0}} = \frac{B_m}{e^{B_m} - 1}, \quad (46)$$

where  $St_{m0}$  denotes the mass Stanton number in the absence of blowing.

Figure 6 presents the concentration of freestream species at the surface,  $1 - c_w$ , plotted against the mass flux  $\dot{m}$ . Note that by inspection of Eqs. (45) and (46),  $\frac{St_m}{St_{m0}} = 1 - c_w$ .  $c_w$  was obtained numerically using the self-similar equations.

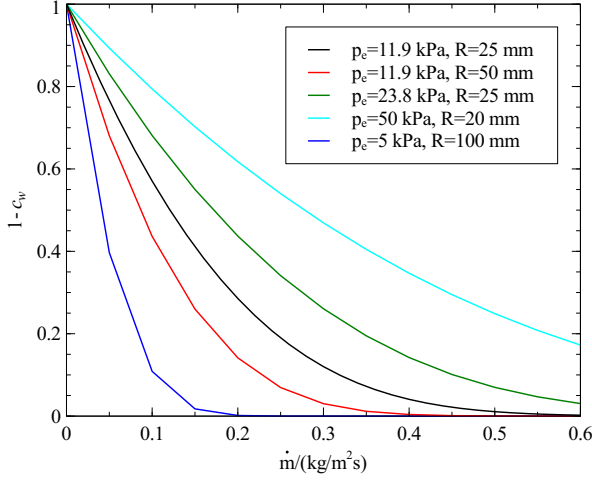


**Fig. 6** Effect of pressure and nose radius for air injection in air at  $T_w = 300K$  and  $T_e = 537K$ .

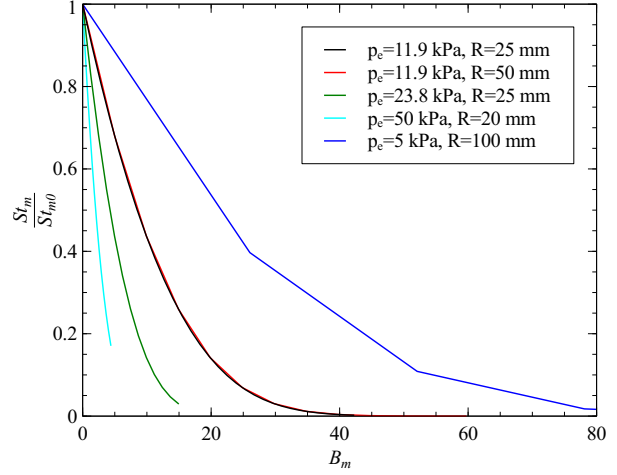


**Fig. 7** Effect of pressure and nose radius for air injection in air at  $T_w = 300K$  and  $T_e = 537K$ .

Intuitively, smaller nose radii and higher boundary layer edge pressures increase the concentration of freestream species at the wall. It is desirable to replace  $\dot{m}$  by a quantity that makes the data collapse.

The blowing parameter for mass transfer,  $B_m = \frac{F}{S_{t_{m0}}}$  presents itself as an obvious candidate. However, as can be seen in Fig. 7, the data does not collapse satisfactorily. Despite the narrow subset of cases with constant gas and temperature,  $B_m = \frac{F}{S_{t_{m0}}}$  alone does not seem to be a good predictor for the ratio of mass Stanton numbers. It corrects for the geometry, specifically the nose radius, but not for the boundary layer edge pressure. The correction factor presented in Eq. (3), yielding  $B_{m,1} = \lambda_1 B_m$  does not provide a satisfactory fit either. All cases considered in Fig. 7 involve air injection into an air freestream, thus  $\lambda_1 = 1$ . The aim of this paper is to improve this scaling factor  $\lambda$ .

### III. Parameter Scaling and Results

The aim of this section is to derive a scaling factor  $\lambda$  analytically, starting with the self-similar governing equations for a laminar boundary layer in thermochemical equilibrium. Neglecting the third term (mass generation) of Eq. (13), which is found to be small compared to the first (advection) and the second term (diffusion), one obtains

$$\frac{d^2 c}{d\eta^2} + \frac{f + \frac{\partial \alpha}{\partial \eta}}{\alpha} \left( \frac{dc}{d\eta} \right) = 0, \quad (47)$$

$\beta$  and  $m$  are now defined such that the boundary conditions described after Eq. (41) are met. Note that the coolant concentration,  $c_e$ , is assumed to be zero at the boundary layer edge. Defining  $m = \frac{\eta}{\Delta}$  and  $\beta = \frac{c - c_w}{c_e - c_w} = 1 - \frac{c}{c_w}$  one obtains

$$\frac{d^2 \beta}{dm^2} + \frac{f + \frac{\partial \alpha}{\partial \eta}}{\alpha} \Delta \left( \frac{d\beta}{dm} \right) = 0. \quad (48)$$



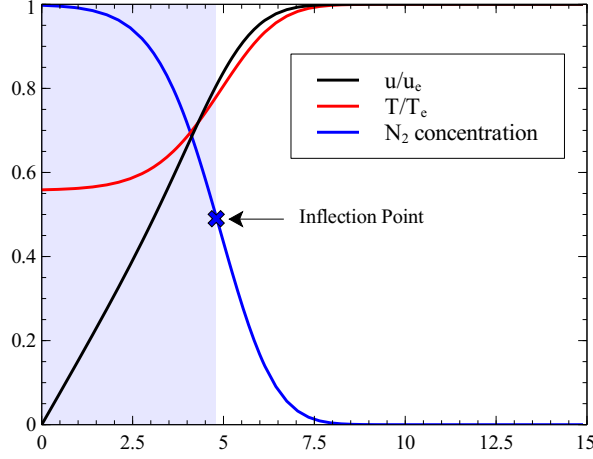


**Fig. 8 Velocity, temperature and concentration profiles for the condition shown in Table 3.**

**Table 3 Input parameters of the reference test case.**

M	$p_e/\text{kPa}$	$T_w/\text{K}$	$T_e/\text{K}$	$\dot{m}/(\frac{\text{kg}}{\text{m}^2\text{s}})$	R/mm
7	11.9	300	537	0.6	25

By comparison with Eq. (41), it is clear that the dimensionless measure of mass transfer rate in the present case is

$$B_m = -\frac{f + \frac{\partial \alpha}{\partial \eta}}{\alpha} \Delta. \quad (49)$$

The first observation is that  $B_m$  is directly proportional to the effective film thickness,  $\Delta$ . It is defined as the thickness of a laminar fluid, which would offer the experimentally observed resistance to the transport of freestream gas to the wall. Thus far, however, there is no expression relating the effective film thickness to known quantities, such as freestream, coolant and geometrical parameters.

Figure 8 presents the numerically obtained self-similar profiles for a Mach 7,  $T_w = 300 \text{ K}$ ,  $T_e = 537 \text{ K}$ ,  $p_e = 11.9 \text{ kPa}$  freestream condition and will be used to illustrate the steps and assumptions made in the following analytical treatment. In this work, the following assumption is made:  $\Delta$  is proportional to the area under the concentration curve in Fig. 8. After all, this area could be redistributed into a rectangular shape, with 100% coolant gas concentration inside and 0% outside of it, thus representing the effective coolant gas film thickness. Observing Fig. 8, it is found that this area can be approximated by a rectangle spanning from zero to the inflection point of the concentration profile. Looking at Eq. (13) this observation is no coincidence. Applying the chain rule and dropping the mass generation term, which is zero away from the wall, one obtains

$$\left(\frac{l}{Sc}\right)c'' = -\left(\frac{l}{Sc}\right)'c' - fc' = 0. \quad (50)$$

Clearly,  $c'$  is not zero at the inflection point, thus the condition is only satisfied if

$$f = \left( \frac{l}{Sc} \right)' \approx 0. \quad (51)$$

The assumption that the gradient  $\left( \frac{l}{Sc} \right)' \approx 0$  at the inflection point was found to be valid through a numerical parameter study. This will change if the injected and freestream gases have significantly different molar masses - an increase in complexity that will be considered in section III.C. Note that from the definition of  $f$  (Eq. (19)), the position of the inflection point coincides with the distance from the wall, at which the velocity,  $v$  changes from being positive (flow moving away from the wall) to negative (flow moving towards the wall). In other words, the concentration layer thickness coincides with the distance away from the wall at which the injected momentum and the freestream momentum balance each other out. In order to find that position it is necessary to derive an expression for  $f$ . In Fig. 8 one can see that the velocity profile between the wall and the inflection point is approximately linear. Thus,  $f$ , which is required to solve Eq. (51), can be approximated as

$$f(\eta) = \int_0^\eta f' d\eta = \int_0^\eta f_w'' \eta d\eta = f_w'' \frac{\eta^2}{2} + f_w. \quad (52)$$

It remains to find an expression for the velocity gradient,  $f_w''$ , at the wall. After applying the no-slip condition, Eq. (11) at the wall reduces to

$$f_w'' = -\frac{(0.5\delta_w + l f_w''')}{(f_w + l'_w)} \approx -\frac{\delta_w}{2f_w}, \quad (53)$$

noting that  $l f_w''' \ll 0.5\delta_w$  and  $l'_w \ll f_w$ . Finally, the position of the inflection point is obtained by finding the root of  $f$ . Combining Eqs. (52) and (53) one obtains

$$f(\eta) = -\frac{\delta_w}{2f_w} \frac{\eta^2}{2} + f_w = 0 \quad (54)$$

and thus for the root:

$$\eta_{c''=0} = \sqrt{\frac{-2f_w}{f_w''}} = \sqrt{\frac{2}{\rho_e \mu_e \frac{du_e}{dx} \delta_w}} \dot{m}. \quad (55)$$

The effective film thickness then becomes

$$\Delta = \eta_{c''=0} = \sqrt{\frac{2}{\rho_e \mu_e \frac{du_e}{dx} \delta_w}} \dot{m}. \quad (56)$$

Following the assumption made in this work, that the blowing parameter is proportional to  $\Delta$ , the results were plotted

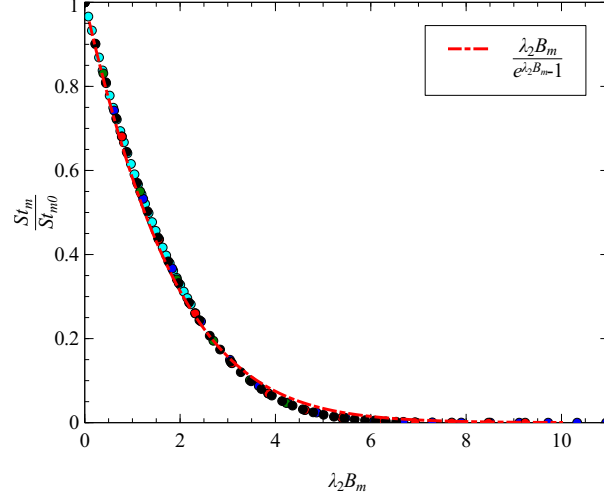


**Fig. 9** All cases from Fig. 6 plotted against  $B_{m,2}$ .

against  $B_{m,2} = 1.29\Delta$  in Fig. 9. In fact, it is found that cases with different freestream pressures and nose radii all collapse onto the same line when plotted against  $B_{m,2} = 1.29\Delta$ , confirming this analytical relationship (Eq. (49)). Using the definition of  $\Delta$  (Eq. (56)) and  $St_{m0}$  (Eq. (40)), one can also express  $B_{m,2}$  as follows:

$$\lambda_2 = 1.625 \left( \frac{\mu_e}{\mu_w} \right)^{0.5} \rho_e \quad (57)$$

$$B_{m,2} = \lambda_2 B_m = \lambda_2 \frac{F}{St_{m0}}. \quad (58)$$

Using thin film theory, it was thus possible to derive the scaling factor for  $B_m$  that is required to obtain a good fit. The aim of the next part is to refine Eq. (57). The factor of 1.625 is unique to the cases considered in Figs. 6 and 9. Currently, it must be obtained numerically each time one of the input parameters, such as  $T_w$ , is changed. It is much more desirable to have an analytical expression of  $T_w$  and all other relevant quantities,  $Fn(T_w, \dots)$ , which covers the full parameter space and provides the  $K_m$  ratio for every flight scenario. Equation (49) suggests that an analytical correlation for the mass transfer rate  $B_m$  is a function of the Schmidt number, the Chapman-Rubesin factor and the blowing parameter:

$$B_m = \Delta \times Fn(Sc, l, f). \quad (59)$$

#### A. Schmidt number scaling

The dependence on  $Sc$ ,  $l$  and  $f$  is found by gradually increasing the complexity of the considered cases. The most simple case is air injection into an air freestream with constant temperature throughout the boundary layer. Thus,

**Table 4 Legend of cases considered in Figs. 10 and 11.**

#	Inj	Ext	$T_w/K$	$T_e/K$	$Sc_w$
1	Air	Air	300	300	0.774
2	Ar	Ar	300	300	0.765
3	$CO_2$	$CO_2$	300	300	0.432
4	He	He	300	300	0.745
5	Ne	Ne	300	300	0.761
6	Xe	Xe	300	300	0.754
7	$N_2$	Air	2000	2000	0.768
8	$N_2$	Air	4000	4000	0.776
9	$N_2$	Air	6000	6000	0.907
10	$N_2$	Air	8000	8000	1.381
11	$N_2$	Air	10000	10000	1.446
12	$N_2$	Air	12000	12000	1.348

$l = \frac{\rho\mu}{\rho_e\mu_e}$  is constant. By comparing cases with constant  $f$ ,  $\lambda_3$  is now merely a function of Schmidt number if Eq. (59) holds true. Figure 10 depicts the numerically obtained mass fraction of external gas at the wall against the previously derived  $B_{m,2} = \lambda_2 B_m$ . In addition, it compares it to the surface concentration computed by Eq. (45). It is apparent that all data points collapse if stretched by a factor  $\lambda_3 = \lambda_2 \times Fn(Sc)$ . More specifically, this factor is found to be  $2Sc_w^{0.6}$ , as illustrated in Fig. 11. The Schmidt number describes the ratio of momentum diffusivity, characterized by the dynamic viscosity  $\frac{\mu}{\rho}$ , to mass diffusivity, linked to the diffusion coefficient,  $D$ . Particles with low  $Sc$  are very volatile, having a high mass diffusivity and low viscous forces holding them back. It is intuitive that for the same effective film thickness,  $\Delta$ , coolants with low  $Sc$  provide a weaker barrier against mass transfer from the external flow to the surface. Thus the factor  $\lambda_3 = \lambda_2 \times 2Sc_w^{0.6}$  does not only provide an excellent fit, but can also be explained physically. It is important to point out that a slight mismatch persists, because  $\lambda_3$  is not derived fully analytically anymore, but semi-empirically instead. A heat-mass transfer analogy is found in Eq. (23) of Ref. [27], where the heat transfer is found to scale with  $Pr^{0.6}$ .

## B. Temperature scaling

The next increment in complexity consists of allowing temperature differences in the boundary layer. Figure 12 shows various numerical results plotted against  $B_{m,3} = \lambda_3 B_m$ . It is apparent that the ratio of boundary layer edge temperature to wall temperature has an effect on the results. More specifically, Fig. 13 shows that the data collapses if  $B_m$  is stretched by the scaling factor  $\lambda_4 = \lambda_3 \times \sqrt{\frac{T_w}{T_e}}$ , thus

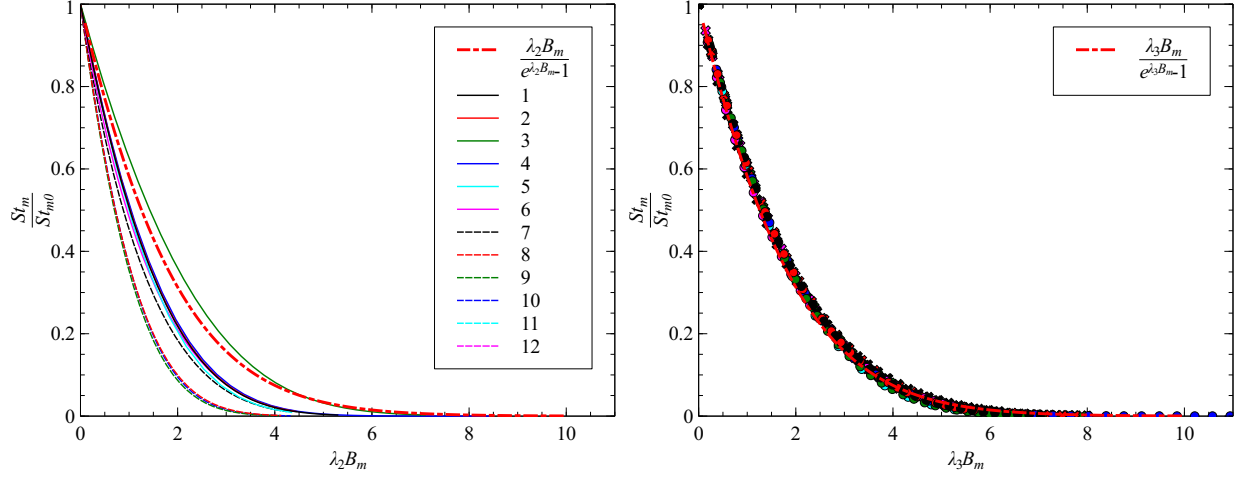


**Fig. 10** Mass fraction of external gas at the wall for Fig. 11 Cases shown in Fig. 10, plotted against  $B_{m,3}$ . cases with varying Schmidt numbers, plotted against  $B_{m,2}$ . A legend is provided in Table 4.

**Table 5** Legend of cases considered in Figs. 12 and 13.

#	Inj	Ext	$T_w/K$	$T_e/K$
1	$N_2$	Air	300	537
2	$N_2$	Air	300	2000
3	$CO_2$	$CO_2$	300	2000
4	$N_2$	Air	300	3000
5	$N_2$	Air	1428	6180

$$\lambda_4 = \left( \frac{\mu_e T_w}{\mu_w T_e} \right)^{0.5} Sc_w^{0.6} 2.52 \rho_e \quad (60)$$

$$B_{m,4} = \lambda_4 B_m \quad (61)$$

### C. Foreign gas injection

Note that even though nitrogen and air dissociate at slightly different temperatures, the difference is minor enough to consider them to be the same gas and thus use  $\lambda_4$  (Eq. (60)) even beyond 2500 K. If the injected and freestream gases are very dissimilar, for instance in a helium cooled stagnation point in a  $CO_2$  freestream, the above theory does not hold. First of all, the assumption made in Eq. (51) becomes invalid, because the gas property gradients affecting  $l'$  and  $Sc'$  are too large. Secondly, the concentration profile such as the one shown in Fig. 8 becomes skewed. In other words,

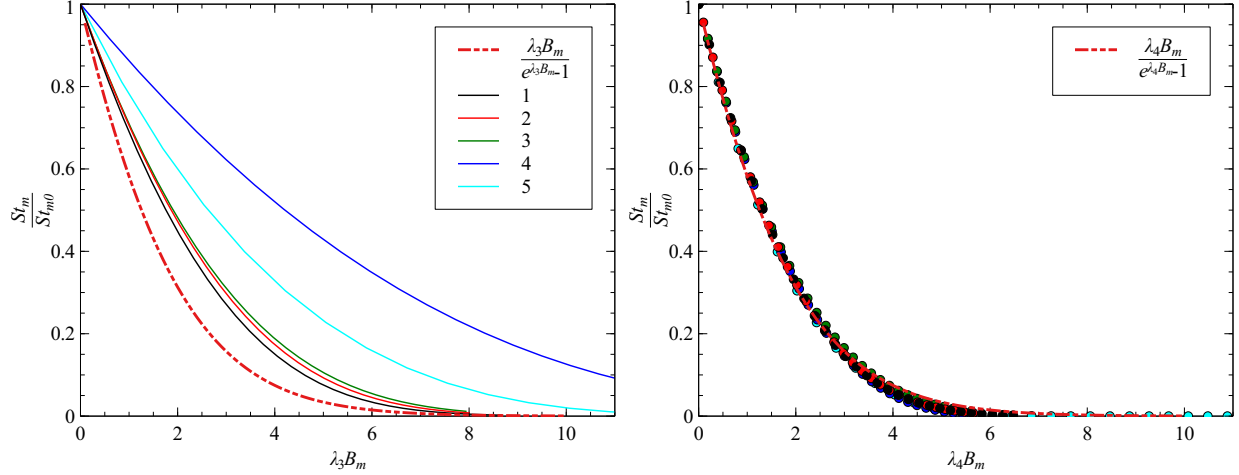


**Fig. 12** Mass fraction of external gas at the wall for Fig. 13 cases with varying wall and boundary layer edge temperatures, plotted against  $B_{m,3}$ . A legend is provided in Table 5.

the inflection point ceases to correlate with the area under the curve. However, combining the following qualitative arguments with numerical observations, it was possible to amend the mass transfer parameter, to provide accurate results even for very dissimilar gases. Considering the hypothetical case of helium injection into a  $\text{CO}_2$  freestream, encountered for instance during a Mars descent, the first step would be to obtain the effective film thickness assuming the coolant to equal the freestream gas, in this case  $\text{CO}_2$ . A qualitative argument can be made about the performance of other coolants relative to  $\text{CO}_2$ . A coolant with a higher mass diffusivity is more volatile and will diffuse into the freestream more quickly, thus providing less protection to the surface. However, this is not the full picture. Since gases are compared for a constant mass injection  $\dot{m}$  at the wall, the quantity of interest should not be just the diffusivity, but the diffusive mass transfer, in other words how much mass per second diffuses into the freestream. A good approximation is given by multiplying the diffusivity by the density at the wall,  $\rho D$ . Since the above qualitative argument is just relative to the freestream gas, in this case  $\text{CO}_2$ , the scaling factor for any other coolant must directly relate to it and is found to be in the form of a ratio:

$$\left( \frac{M_{\text{ext}} D_{\text{ext-ext}}}{M D_{\text{inj-ext}}} \right)_w, \quad (62)$$

noting that  $T_w$  and  $p_w$  will not be affected by the coolant gas change and thus  $\left( \frac{\rho_{\text{ext}}}{\rho} \right)_w = \left( \frac{M_{\text{ext}}}{M} \right)_w$ . In fact, Figs. 14 and 15 show how cases ranging from 300 - 6180K, various pressures, stagnation point radii and eight different gases all collapse if the following final scaling factor is applied:

**Table 6 Legend of cases considered in Figs. 14 and 15.**

#	Inj	Ext	$T_e/\text{K}$	$T_w/\text{K}$	$p_e/\text{kPa}$	$R/\text{mm}$
1	Kr	Air	1790	1000	5	100
2	Ar	Air	1790	1000	5	100
3	Ar	Air	6180	1428	3.2	25
4	He	Air	6180	1428	11.9	25
5	N <sub>2</sub>	CO <sub>2</sub>	2000	1000	11.9	25
6	Ne	Ne	300	300	11.9	25
7	Xe	Xe	300	300	11.9	25
8	N <sub>2</sub>	Air	1800	1000	100	1000
9	N <sub>2</sub>	Air	3000	1000	200	1000

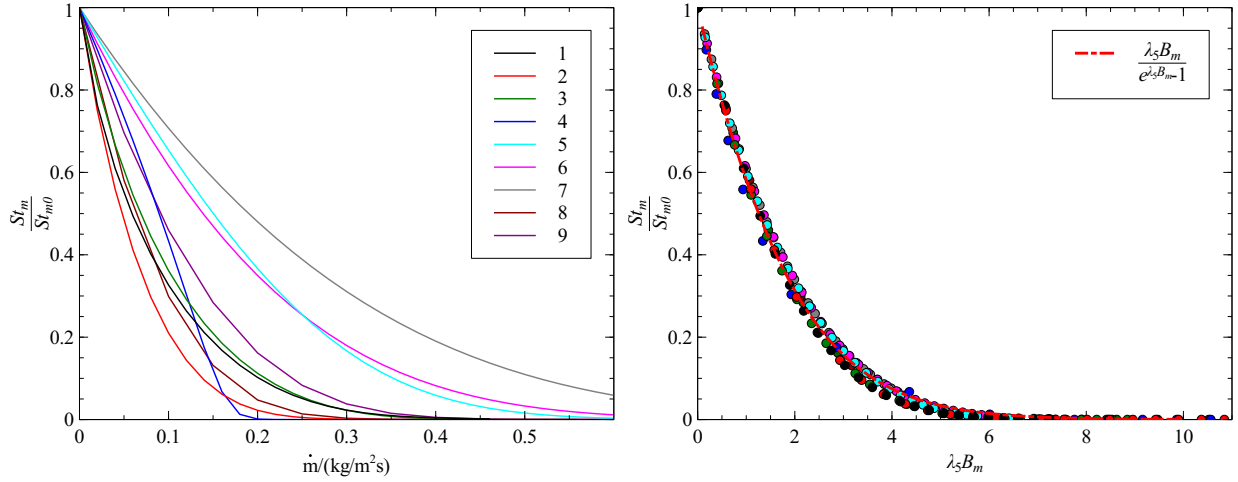


**Fig. 14 Cases described in Table 6 plotted against the mass flow rate at the wall.**

**Fig. 15 Cases described in Table 6 plotted against the blowing parameter presented in this paper.**

$$\lambda_5 = \lambda_4 \times \left( \frac{M_{\text{ext}} D_{\text{ext-ext}}}{M D_{\text{inj-ext}}} \right)_w^{0.75} \quad (63)$$

$$B_{m,5} = \lambda_5 B_m \quad (64)$$

$$1 - c_w = \frac{B_{m,5}}{e^{B_{m,5}} - 1} \quad (65)$$

where inj and ext denote the injected and external gas type. Note that  $M_w = Fn(c_w)$ , thus making the expression implicit. However, the solution is unique and converges. Generally two or three iterations are sufficient to be within 0.5% of the fully converged result for very dissimilar gases. One starts with an initial guess for  $c_w$  and then applies Eq. (63) and Eq. (65) in alternation to update  $B_{m,5}$  and  $c_w$ , respectively. Alternatively, using the definitions of  $F$  and  $St_0$ ,

$B_{m,5}$  can be expressed as follows:

$$B_{m,5} = \sqrt{\frac{8}{\rho_e \mu_e \frac{du_e}{dx}}} Sc_{w:\text{ext}}^{0.6} \dot{m} \left( \frac{M_{\text{ext}} D_{\text{ext-ext}}}{M D_{\text{inj-ext}}} \right)_w^{0.75}. \quad (66)$$

This formulation combines the effects of boundary layer edge pressure and temperature, nose radius, wall temperature, freestream species Schmidt number, injected mass flow rate, as well as foreign gas injection.

## IV. Discussion

Analogous to the blowing parameter with respect to heat transfer  $B_h$ ,  $B_m$  can now be used for flight to ground scaling. Similar to Kolesnikov's [28] Local Heat Transfer Simulation, used to replicate in-flight heat fluxes in ground facilities, this work presents the concept of Local Surface Concentration Simulation. The wall concentration of external flow or equivalently the ratio of mass Stanton numbers, will be the same as long as the  $B_m$  parameter is matched. In an air freestream which is in thermal and chemical equilibrium,  $B_m$  is only a function of  $p_e$ ,  $T_e$ ,  $\frac{du_e}{dx}$ ,  $T_w$ ,  $\dot{m}$  as well as the two coolant properties  $M_{\text{inj}}$  and  $D_{\text{inj-ext}}$ . Inspection of Eq. (66) further reveals that the best foreign gas is the one with the smallest  $M D_{\text{inj-ext}}$  term and not just  $M$  as suggested by Eq. (3). Best protection, for a given  $\dot{m}$ , is thus provided by a light gas with low mass diffusivity. Helium has a relatively high diffusivity and is thus sometimes outperformed by nitrogen. Note, however, that a boundary layer with large amounts of helium injection ceases to be self-similar and thus the correlation presented in this paper cannot be used. This is also true for other extremely light gases, such as hydrogen. This is because the  $\frac{u_e^2}{h_e} \ll 1$  assumption becomes inaccurate. In the full self-similar solutions,  $\frac{u_e^2}{h_e}$  is multiplied with  $\frac{\rho_e}{\rho}$  and  $f''^2$ , both of which become so large for very light gases, that the product cannot be neglected anymore. However, if  $u_e = \frac{\partial u_e}{\partial x} x$  is kept, the solution would depend on  $x$  and thus cannot be solved in a self-similar way. The discrepancies were limited to hydrogen and moderate to large amounts of helium blowing. Boundary layers with injection of heavier gases, such as neon, into air, were all found to be self-similar.

An uncertainty analysis for the representative set of cases considered in this paper (Tables 4 to 6) showed an error of  $\pm 4\%$  or  $\pm 1.5$  percentage points, whichever is greater. The method presented in this work can be used with any freestream gas and for high-temperature cases, as long as the self-similar assumptions listed in section II.A are met. This marks a significant improvement to previous works [16]. Furthermore, it is derived semi-analytically and explicitly reveals the effect of all parameters involved. This makes it a practical tool for early design decisions, such as choosing the blowing rate for a transpiration cooled wall or the flight trajectory of an ablative heat shield. This analytical approximation is also useful for existing oxidation models, such as the one in Ref. [29] for  $\text{ZrB}_2$  at 1273 - 2073K. The chemical rate of reaction is an essential parameter of the model and is directly dependent on the oxygen concentration at the wall. The correlation presented in this paper is also helpful to speed up convergence of high-fidelity numerical simulations by providing an estimate of the surface concentration for a given injection rate. Currently the surface concentration is



computed by balancing the advective and diffusive flux (employing Eq. (25)), which requires many expensive iterations. The modelling used in this paper and matching CFD assumes that the flow is in thermochemical equilibrium. However, some non-equilibrium conditions were chosen deliberately in Table 4 (#8-12), Table 5 (#5) and Table 6 (#3,4). The aim of expanding the range outside of where the equilibrium assumption would hold was to ensure the data still collapsed. Non-equilibrium effects will be explored in future studies.

## V. Conclusion

This paper presents a tool for the design of hypersonic stagnation points with mass injection. It assumes flow in thermochemical equilibrium and can be used with any freestream gas and for high-temperature cases, as long as the self-similar assumptions listed in section II.A are met. Note that boundary layers with hydrogen and helium injection were often found to not be self-similar and can thus not be modeled reliably with this correlation. However, the discrepancy was limited to these two coolants and did not persist for heavier gases, such as Neon. The main advantage of this semi-analytically derived method over numerical solvers is that it explicitly reveals the effect of each component in the parameter space. It was validated against the numerically obtained self-similar solutions and featured an error of  $\pm 4$  percent or  $\pm 1.5$  percentage points, whichever is greater. However, similar to the Fay-Riddell heat transfer prediction, it is not intended to provide perfect accuracy, but instead to aid early design decisions, such as the choice of coolant, the nose radius or the rate of mass injection. The method is also very useful for flight to ground scaling of surface concentrations and mass Stanton numbers. In addition, it can complement existing theoretical oxidation models, by providing a concentration value and thus the oxygen partial pressure for a real flight condition, which directly affects the chemical rate of reaction. Furthermore, it can be employed to provide an initial  $c_w$  guess for numerical models to speed up convergence. Future tests are planned to validate this method experimentally in a hypersonic flow facility.

## Funding Sources

This research is funded by the EPSRC grant "Transpiration Cooling Systems for Jet Engine Turbines and Hypersonic Flight" (EP/P000878/1).

## Acknowledgments

The authors of this paper gratefully acknowledge the assistance of Peter Jacobs with Eilmer 4 and the helpful comments from Jim Merrifield and Stefan Loehle.

## References

- [1] Heppenheimer, T. A., *Facing the heat barrier: a history of hypersonics*, Vol. 4232, Government Printing Office, 2009.
- [2] Fay, J. A., and Riddell, F. R., "Theory of stagnation point heat transfer in dissociated air," *Journal of the Aerospace Sciences*,

Vol. 25, No. 2, 1958, pp. 73–85. <https://doi.org/10.2514/8.7517>.

- [3] Sutton, K., and Graves Jr, R. A., “A general stagnation-point convective heating equation for arbitrary gas mixtures,” *NASA Technical Report TR R-376*, 1971.
- [4] Kays, W. M., *Convective heat and mass transfer, 3rd ed.*, Tata McGraw-Hill Education, 2012. [https://doi.org/10.1016/0017-9310\(72\)90237-2](https://doi.org/10.1016/0017-9310(72)90237-2).
- [5] Henline, W. D., “Transpiration cooling of hypersonic blunt bodies with finite rate surface reactions,” *NASA STI/Recon Technical Report N*, Vol. 89, 1989, p. 24580.
- [6] Otsu, H., Fujita, K., and Ito, T., “Application of the transpiration cooling method for reentry vehicles,” *45th AIAA Aerospace Sciences Meeting and Exhibit*, 2007, p. 1209. <https://doi.org/10.2514/6.2007-1209>.
- [7] Hermann, T., McGilvray, M., and Naved, I., “Performance of Transpiration-Cooled Heat Shields for Reentry Vehicles,” *AIAA Journal*, Vol. 58, No. 2, 2020, pp. 830–841. <https://doi.org/10.2514/1.J058515>.
- [8] Loehman, R., Corral, E., Dumm, H. P., Kotula, P., Tandon, R., et al., “Ultrahigh-Temperature Ceramics For Hypersonic Vehicle Applications,” *Industrial Heating*, Vol. 71, No. 1, 2004, pp. 36–38. <https://doi.org/10.2172/887260>.
- [9] Francese, A., “Numerical and experimental study of UHTC materials for atmospheric re-entry,” *Dottorato di ricerca in ingegneria aerospaziale*, 2007.
- [10] Reimer, T., Kuhn, M., Gülhan, A., Esser, B., Sippel, M., and van Foreest, A., “Transpiration cooling tests of porous CMC in hypersonic flow,” *17th AIAA International Space Planes and Hypersonic Systems and Technologies Conference*, 2011, p. 2251. <https://doi.org/10.2514/6.2011-2251>.
- [11] Bacos, M., “Carbon-carbon composites: oxidation behavior and coatings protection,” *Le Journal de Physique IV*, Vol. 3, No. C7, 1993, pp. C7–1895. <https://doi.org/10.1051/jp4:19937303>.
- [12] Kim, I., Park, G., and Na, J. J., “Experimental study of surface roughness effect on oxygen catalytic recombination,” *International Journal of Heat and Mass Transfer*, Vol. 138, 2019, pp. 916–922. <https://doi.org/10.1016/j.ijheatmasstransfer.2019.04.049>.
- [13] Yang, Y., Kim, I., and Park, G., “Experimental and numerical study of oxygen catalytic recombination of SiC-coated material,” *International Journal of Heat and Mass Transfer*, Vol. 143, 2019, p. 118510. <https://doi.org/10.1016/j.ijheatmasstransfer.2019.118510>.
- [14] Steinheuer, J., “Berechnung der laminaren Zweistoff-Grenzschicht in der hypersonischen Staupunktströmung mit temperaturabhängigen Stoffbeiwerten,” *ZAMM-Journal of Applied Mathematics and Mechanics/Zeitschrift für Angewandte Mathematik und Mechanik*, Vol. 51, No. 3, 1971, pp. 209–223. <https://doi.org/10.1007/BF01002178>.
- [15] Mickley, H., Ross, R., Squyers, A., and Stewart, W., “Heat, Mass, and Momentum Transfer for Flow over a Flat Plate with Blowing or Suction,” *National Advisory Committee for Aeronautics*, Vol. 3208, 1954.

- [16] Mills, A., and Wortman, A., “Two-dimensional stagnation point flows of binary mixtures,” *International Journal of Heat and Mass Transfer*, Vol. 15, No. 5, 1972, pp. 969–987. [https://doi.org/10.1016/0017-9310\(72\)90234-7](https://doi.org/10.1016/0017-9310(72)90234-7).
- [17] Anderson Jr, J. D., *Hypersonic and high-temperature gas dynamics*, American Institute of Aeronautics and Astronautics, 2006. <https://doi.org/10.2514/4.105142>.
- [18] Dorodnitsyn, A., “Laminar boundary layer in compressible fluid,” *Dokl. Akad. Nauk SSSR*, Vol. 34, 1942, pp. 213–219.
- [19] Lees, L., “Laminar heat transfer over blunt-nosed bodies at hypersonic flight speeds,” *Journal of Jet Propulsion*, Vol. 26, No. 4, 1956, pp. 259–269. <https://doi.org/10.2514/8.6977>.
- [20] Schlichting, H., and Gersten, K., *Boundary-layer theory*, Springer, 2016. <https://doi.org/10.1007/978-3-662-52919-5>.
- [21] ASTM E637-05(2016), *Standard Test Method for Calculation of Stagnation Enthalpy from Heat Transfer Theory and Experimental Measurements of Stagnation-Point Heat Transfer and Pressure*, ASTM International, West Conshohocken, PA, 2016. <https://doi.org/10.1520/E0637-05R16>.
- [22] Bird, R. B., “Transport phenomena,” *Appl. Mech. Rev.*, Vol. 55, No. 1, 2002, pp. R1–R4. <https://doi.org/10.1021/ed038pA640>.
- [23] Snyder, C., “CEARUN,” , 2012. <https://cearun.grc.nasa.gov>.
- [24] Gollan, R. J., and Jacobs, P., “About the formulation, verification and validation of the hypersonic flow solver Eilmer,” *International Journal for Numerical Methods in Fluids*, Vol. 73, No. 1, 2013, pp. 19–57. <https://doi.org/10.1002/fld.3790>.
- [25] Jacobs, P., and Gollan, R., “Implementation of a compressible-flow simulation code in the D programming language,” *Applied Mechanics and Materials*, Vol. 846, Trans Tech Publ, 2016, pp. 54–60. <https://doi.org/10.4028/www.scientific.net/AMM.846.54>.
- [26] Kays, W. M., “Heat transfer to the transpired turbulent boundary layer,” *International Journal of Heat and Mass Transfer*, Vol. 15, No. 5, 1972, pp. 1023 – 1044. [https://doi.org/10.1016/0017-9310\(72\)90237-2](https://doi.org/10.1016/0017-9310(72)90237-2).
- [27] Van Driest, E. R., *The problem of aerodynamic heating*, Institute of the Aeronautical Sciences, 1956.
- [28] Kolesnikov, A., “The aerothermodynamic simulation in-and supersonic high-enthalpy jets: experiment and theory,” *Aerothermodynamics for space vehicles*, Vol. 367, 1995, p. 583.
- [29] Parthasarathy, T., Rapp, R., Opeka, M., and Kerans, R., “A model for the oxidation of ZrB<sub>2</sub>, HfB<sub>2</sub> and TiB<sub>2</sub>,” *Acta Materialia*, Vol. 55, No. 17, 2007, pp. 5999–6010. <https://doi.org/10.1016/j.actamat.2007.07.027>.